MAPPING COLORADO RIVER ECOSYSTEM RESOURCES IN GLEN CANYON: ANALYSIS OF HYPERSPECTRAL LOW-ALTITUDE AVIRIS IMAGERY[*]

Erzsébet Merényi
Rice University, Houston, TX (erzsebet@ece.rice.edu)

William H. Farrand
Space Science Institute, Boulder, CO (william.farrand@colorado.edu)

Lawrence E. Stevens
Grand Canyon Wildlands Council, Flagstaff, AZ (farvana@aol.com)

Theodore S. Melis
Grand Canyon Monitoring and Research Center, Flagstaff, AZ (tmelis@flagmail.wr.usgs.gov)

Kapil Chhibber
University of Arizona, NASA Space Grant Program, Tucson, AZ (kapil@u.arizona.edu)

ABSTRACT

We are analyzing low-altitude AVIRIS images for identifying and mapping components of the Colorado River ecosystem. The 2.7 m/pixel spatial resolution and the 10 nm spectral resolution of these images allow the separation of many cover classes that are of interest for resource management purposes. With sensitive analysis tools we map ten vegetation species and groups, five water classes including algae-laden water and underwater sediments, and five soil/rock types. Future refinement is possible with additional field work or by analyzing hyperspectral images with higher spatial resolution. This work is a feasibility study. We demonstrate that hyperspectral remote sensing imagery can be a powerful tool for effective monitoring of a great number of ecosystem resources, and for providing timely information for stakeholders, over large areas.

1.0 MANAGEMENT ISSUES IN THE COLORADO RIVER ECOSYSTEM

Operational impacts of Glen Canyon Dam on downstream resources of the Colorado River ecosystem have been the subject of intense study and discussions among adaptive management stakeholders that include Federal, State and tribal entities, as well as recreational businesses, environmentalists, power companies, and others (U.S. Bureau of Reclamation 1995, Schmidt et al. 1998). The Grand Canyon Monitoring and Research Center (GCMRC within the U.S. Department of Interior) has identified the following key objectives for long-term monitoring of vital components of the ecosystem between Lakes Powell and Mead, while providing stakeholders with information for decision making: 1) lowest possible impact on critical resources; 2) highest possible return of integrated scientific information; and 3) long-term, repeatable data collection. Airborne hyperspectral image data are being considered as a possible long-term monitoring tool, which hold the promise of being able to fulfill the above requirements. This study is a pilot project intended to explore the extent and variety of

[*] Proc. Fourteenth International Conference on Applied Geologic Remote Sensing, Las Vegas, Nevada, 6-8 November 2000, pp 44-51. For color reprint email to erzsebet@ece.rice.edu.

information, relevant for long-term monitoring, that can be extracted from images of both high spectral and spatial resolution.

The Colorado River ecosystem in Glen Canyon and Grand Canyon poses special challenges for remote monitoring with respect to logistics required to support field-based studies and relative to spatial scales at which monitoring is needed. The narrow corridor of the river is confined by tall vertical cliffs, yet provides a habitat for a great variety of both native and non-native plant species. Riparian vegetation consists of stands that often cover only very small areas. Often, these stands consist of intermixed native and non-native species, and spectral signatures of the various plants sometimes display only subtle differences. Adequate change detection mapping requires both high spectral and high spatial resolution, as well as advanced processing algorithms that can detect subtle spectral differences.

Change detection for evolving sand bars, rapids and debris fans is a critical part of the GCMRC's long-term monitoring program. Additionally, changes in the aquatic ecosystem's food base, such as abundance and distribution of algae and other benthic organisms are of great interest. Presently, the need to lower river stage for 2-3 days during annual monitoring overflights for conventional aerial photography and traditional surface measurements introduces artificial and undesirable impacts on the ecosystem (e.g., Blinn et al. 1999). With hyperspectral imagery, we expect to map riparian vegetation, terrestrial sediment deposits, as well as sand bars and benthic organisms through some depth of water, obtaining greater compositional information than can be obtained through the use of aerial photography.

2.0 AVIRISLA DATA AND PREPROCESSING

Low altitude AVIRIS data were collected on October 4, 1998, in two runs. The data set comprises approximately 10 Gigabytes of data, divided into 10 image frames. These frames cover river miles –5.5 to –12.0, about 2.5% of the 300 miles long river corridor between Lake Powell and Lake Mead, and roughly 8% of the GIS study sites monitored by the GCMRC (see Figure 1 of Merényi et al, 2000). The three frames analyzed in this paper contain river miles –5.5 to –8.5, a portion of the river with a wide array of sediment and bedrock types and various typical aquatic and riparian plant assemblages. The spatial resolution is approximately 2.7 m/pixel. North is shown at approximately ten –o'clock, and the river flows top to bottom in the frames. All four AVIRIS spectrometers functioned properly during the October 4 data acquisition. On 21 and 22 August 1998, field spectra of over 70 soil, rock and vegetation species were collected with an ASD FieldSpec FR, in areas that fall within our AVIRISLA image frames. A portion of these field spectra along with field photos of the respective species are posted at Hhttp://www.lpl.arizona.edu/~erzsebet/index.html , under "Ecosystem".

The images received from the AVIRIS data lab had been geometrically rectified and registered (Boardman, 1999) and calibrated to at-sensor radiance. The image data were then converted to apparent surface reflectance through the use of the ATREM program (Gao et al., 1993). In order to remove residual instrumental and atmospheric effects remaining after the ATREM correction, a second stage "modified flat field" (Farrand, 1992) correction was applied. This second stage correction consisted of the following steps: first, an average spectrum of three pixels covering a quartz sand bar that was visited during the August, 1998 field work was calculated. This average ATREM corrected spectrum was divided into each pixel in the ATREM corrected data cube, then each pixel spectrum was multiplied through by a smoothed field spectrum of the sand bar. Further preprocessing included trimming off the no-data fringes, and elimination of the overlapping and excessively noisy bands, leaving 194 image bands. Before classification, a normalization (as described in Merényi et al., 1996) was also applied in order to cancel linear (i.e. terrain induced) shading effects. This treatment eliminates albedo differences; however, the benefits of normalization outweigh the disadvantages in most applications.

3.0 IMAGE ANALYSES

Two independent analyses were performed: supervised classification by an Artificial Neural Network and Spectral Mixture Analysis. These are presented in Figures 1.a and 1.b, respectively.The three AVIRIS scenes, 4, 5 and 6, are shown from top to bottom in the figures. The results were evaluated against field data that the GCMRC has accumulated over 20 years, against field spectra that were collected in August, 1998, and against the field knowledge of co-authors LS and TM. They have up-to-date, detailed knowledge of the spatial distribution of the resources mapped in this work, through their regular visits to the field (e.g., Stevens et al., 1995, 1997; Kaplinski et al., 1999).

3.1 RESULTS OF ARTIFICIAL NEURAL NETWORK CLASSIFICATION

In this work, we improved and extended the results of Merényi et al. (2000). The number of surface cover types distinguished is 21 in comparison to 18 in the earlier study, and we used three adjacent AVIRIS frames for a larger coverage and statistics. The hybrid Artificial Neural Net (ANN) paradigm, which contains a Self-Organizing Map, is described in detail in Merényi et al. (1997), and Merényi (1998). For this task, 194 input neurons (corresponding to the number of spectral channels), a 40 x 40 hidden Self-Organizing layer, and 21 output neurons (one for each class) were applied. The software used is a collection of NeuralWare (1993) based classifiers and Khoros (Rasure and Young, 1992) based data exploration and other supporting tools, developed for hyperspectral imagery by EM under NASA support. The classes for which to train were determined on the basis of spectral variability found in the image. Identification of the spectral types (labeling the classes) was done by comparison to field spectra, and with the help of co-author LS. The resulting class map is shown in Figure 1.a., with details enlarged in Figures 2.a and 2.b. Mean spectra of classes are presented in Figure 3.

The greater surroundings of the river corridor in the section covered by our three AVIRIS frames are dominated by red and white Navajo sandstone, which is mapped as class O and class N. Class O coincides with nearly vertical cliffs where dark MnO_2 coating ("desert varnish") is common. Shading is also severe here due to the extreme geometry and it may cause as yet uninterpreted spectral effects. Indeed, the composition of classes O and N is the same but the spectral signatures exhibit systematic differences that could be the result of the extreme geometry. Class Q appears to be red sandstone where strong leaching of iron oxides has occurred. White alluvial and eolian sand (class P) is present in small sand beaches along the river. White sand is also exposed in the upper riparian zone (above the "old high water line"), which was the 10 yr, pre-dam flood stage elevation), and it has been detected by this classification. The most obvious example is the nearly horizontal white linear feature toward the right side of scene 6, just above the bank at the inner curve of the river. In addition, white sand appears interspersed with the buff colored Navajo sandstone (Q) at the left of frames 5 and 6, as well as at the right toward the middle of frame 6. Part of those occurrences is indeed loose white sand that accumulates in valleys, and part of it is exposed white sandstone bedrock, which is the source for the loose white sand in the area.

The water in these images has two significantly different segments. Class M shows no spectral signature of sediments. The water in sections M is deep or very darkened by the shadows cast by the vertical cliffs. For example, in scene 6, the water is deep along the left shore (right in the image, close to the vertical cliff classified as N), and obscures the sediments. The water is not very deep on the right side, however, the very tall cliffs cast shadows even at local noon when this image was taken, and further degrade the spectra. These effects will have to be investigated and calibrated. The river segment downstream of class M (downstream of the sharp diagonal dividing line at the cliff's base near the center of image 6) is less deep on either side with no shadows cast on it. In this part, clear signatures of fine sediments (mainly sand) have been detected through the water. Similar details can be pointed out in frames 4 and 5. We attempted to map submerged sediments in three broad categories here: sediments under "shallow" water, under "deeper" water, and in the "deepest" part of the water. Class J represents sand banks under very shallow water. Training samples for this class were taken from the "L" shaped large sand bank close to the white sand beach just downstream of the dividing line of class M (Figure 2.a). Note that a very small sand bank close to the left shore, under shallow water, was detected in the "deep water" (M) section (Figure 2.b). Classes K and L map submerged sediments under two additional, progressively deepening water levels.

Algae-laden water, mapped as class I, corresponds well to known locations of shallow algal colonies, in distinct elongated patches along the shoreline.

Ten vegetation classes were separated. Redbud (*Cercis occidentalis*), a native tree, which grows in protected crevices up in the cliffs and away from the river (class F), a mixture of other upland plants (class S), a mixture of riparian plants (U), six riparian species, and two soil/rock/vegetation classes (T and H). With the exception of redbud, these are all represented on the sand beach in Figure 2.b, which was one of the sites for our fieldwork in August, 1998. Monitoring the spatial distribution of these species is an important management goal as they make up the bulk of riparian habitat used by invertebrate and vertebrate fauna, and their distribution indicates or forecasts change in the ecosystem induced by variation in the flow regime or new (artificially introduced) components or by other factors (Stevens 1989). Tamarisk (*Tamarix ramosissima*), a widespread, non-native tree, is mapped as class A, and matches the known, relatively large plant stands in these images. Arrowweed (*Tessaria*

sericea, class B), partially decayed in the fall, and "Mixed grass" (primarily *Bromus* spp. and *Sporobolus* spp., class E) were recognized and mapped based on their field spectra, and generally correspond to ground truth, showing along shorelines. Training samples for coyote willow (*Salix exigua*, C), watersedge (*Carex aquatilis*, D), and seep willow (*Baccharis emor*yi and *B. salicifolia*, G) were identified from the site of our fieldwork (Figure 2.b) by our domain expert LS. The seep willow (G, maroon) on a sand bar, wedged diagonally into the large, 50-60 m wide, tamarisk stand and flanked by grass and coyote willows, is perfectly mapped. The main coyote willow stand just above and to the left of the white sand beach in Figure 1.b is mapped faithfully, as is the watersedge colony (D, dark green) along a backwater. A mixture of deciduous riparian shrubs such as rabbitbrush (*Chrysothamnus nauseosus*), snakeweed (*Gutierrezia sarothrae*), and Emory seep willow comprise class U (turqoise). These plants are either very similar to each other in their spectral signatures, or grow in too small stands to separate them in the 2.7 m pixels. Class S contains a mix of upland deciduous plants, such as *Isocoma drummondi* (a small, semi-riparian shrub species similar to rabbitbrush), drop seed grasses (*Sporobolus* ssp.). Rabbitbrush and snakeweed, which grow in upland areas too, can also be part of this mix. Class S shows exactly where expected: bordering the riparian vegetation stands toward the hill slopes. Two remaining vegetation classes are mixed: sparse vegetation on sand is shown as class T (medium gray), typically bordering the densely vegetated patches toward the slopes. Grassy talus slope (H, orange) shows at the right locations, from the edges of vegetated patches up the slopes, more abundant in drainages than elsewhere. This class exhibits both rock and grass signatures. Class R is as yet unidentified material. Unclassified pixels cover 19% of the area. These are due to insufficient sampling of classes where continuous changeover takes place between two cover types, or due to materials that may have remained unrecognized as separate species.Evaluation of unclassified pixels can result in further improvement of the class map.

3.2 SPECTRAL MIXTURE ANALYSIS AND SAM MAPPING

Another approach considered here was using processing tools resident in the ENVI software package (RSI, 1997). Each scene was processed seperately although some endmembers from a given scene were used in more than one scene. Each scene was transformed using a Minimum Noise Fraction (MNF) transform. Then, a small number of endmembers were determined by examining two dimensional scatterplots in which the first several MNF bands were successively plotted against each other and pixels at the vertices of the observed data clouds were selected. Using averages of these pixels, the data were reduced via Spectral Mixture Analysis (SMA) (Adams et al., 1993). Since each scene was compositionally similar, each could be well modeled by a set of three endmembers: a "white" (relatively ferric oxide free) rock, a "red" (ferric oxide – rich) rock, and green vegetation. From the RMS error image, a number of spatially restricted materials were identified including white sand beaches and submerged sediments. A region of interest (ROI) was defined by thresholding the vegetation fraction image. The first six MNF bands were interactively examined with the ENVI n-dimensional visualization tool using the vegetation-rich pixels as the input ROI. In this way, a number of distinct vegetation classes were identified. Several of the more spectrally distinct vegetation classes along with the two rock endmembers and the "submerged sediments" and "white sand" materials (identified in the SMA RMS error image) were used as the target materials for a Spectral Angle Mapper (SAM) classification that is presented in Figure 1.b.

In scene 6, the species mapped by SAM classification included three terrestrial vegetation types, three rock/soil types and two "in-water"species. Classes 1, 2 and 4 mostly match the coyote willow, arrow weed, and tamarisk, respectively, in the ANN classification (Figure 1.a). Classes 5, 6, and 7 are the same as classes O, N, and P in Figure 2. Class 3 appears to coincide with class R of the ANN map, and class 8 does not match any of the ANN classes. In scene 5, two rock types were mapped, a submerged sediment class was included, but did not exceed the SAM threshold for inclusion in the class map and four vegetation types were mapped. In scene 4, the submerged sediment was mapped as well as two rock types and four vegetation types..

4.0 SUMMARY OF RESULTS, AND FUTURE IMPROVEMENTS

The remote sensing and analysis approaches used here show great promise for ecosystem monitoring in Grand Canyon, and elsewhere. Further refinement of these techniques, combined with GIS technology, will provide a basis for expanding the scope of coverage to other GIS reaches of the GCMRC, which are presently being

monitored through costly, intrusive, on-the-ground approaches. These techniques offer important new analytical tools for evaluating and monitoring other ecosystems, on earth and elsewhere.

We mapped ten vegetation species, 5 "in-water" species such as algae plus submerged sediments, and five rock/soil types from a low-altitude AVIRIS image covering the –5.5 to –8.5 river miles of the Colorado River in Glen Canyon. The 2.7 m/px spatial resolution allowed very detailed mapping of plant stands that are important to distinguish and monitor, on the few meters scale. The presented analyses are in good agreement with ground truth In this first attempt we achieved a goal of mapping underwater sediments, with a qualitative distinction among three levels of water covering the sediments. As resources allow, future work will include more gradations, and more quantitative assessment of water depth and distinguishing among sand, cobbles and other materials underwater.

The area covered represents a significant statistical basis for the evaluation of the powers of high spatial resolution hyperspectral imaging as a potential monitoring approach. For example, this canyon-bound river reach demonstrates an intriguing geomorphic characteristic that is obvious only through remote sensing analyses. In alluvial rivers, erosion is characteristic on the outside bends, and deposition characterizes the inside bends. That process may be equivocal or reversed in canyon-bound rivers. For example, in frame 6, deposition and vegetation development are conspicuous on the outside of the bend at -6 Mile (lower boxed area). Quantitative assessment of the area coverage of vegetation supports this observation. Once an acceptable classification is produced, the extent of vegetation cover can simply be calculated by multiplying the number of pixels in the vegetation classes by the pixel area, in this case by 2.7 x 2.7 square meters. From a refined classification such as presented in Figure 1.a, the vegetated area can also be broken down to coverage by the individual classes. In scene 6, the vegetation cover calculated this way is approximately 156,000 m^2 along 1 river mile. Tamarisk occupies ~14,000 m^2, and other riparian vegetation covers ~ 36,000 $m^{2.}$ These are rough estimates since there is some small amount of sparse vegetation farther away from the river banks. However, the contribution from those pixels should be too small to significantly change the above estimate. For better accuracy, georegistration and precise masking of the shoreline, as well as accounting for the sampling uncertainty of AVIRISLA will be done in future work.

Resources permitting, 1.5 m/pixel HYDICE imagery, obtained by the GCMRC nearly concurrently with these AVIRIS images , could also be analyzed to achieve higher accuracy. The HYDICE imagery covers the areas presented here, as well as a downstream reach (river mile +7.9) where more terrestrial features with coarse sediment textures, such as debris fans and rapids can be studied.

5.0 ACKNOWLEDGEMENTS

EM is funded for development of neural net tools by NASA, OSSA Applied Information Systems Research Program, NAG54001. KCh is supported by NASA's Space Grant Program. The Grand Canyon Monitoring and Research Center provided all support for the August, 1998 field work, and we thank M. Liszewski and his staff for field assistance. Further field studies by LS and EM were part of a research raft trip, supported by GCMRC and the National Park Service. The ASD FieldSpec FR instrument and expertese were graciously provided by the Remote Sensing Group of the University of Arizona. The authors are grateful to the JPL AVIRIS team for collecting and making available the geometrically reconstructed low-altitude AVIRIS imagery.

6.0 REFERENCES

Adams, J.B., M.O. Smith, and A.R. Gillespie, 1993, "Imaging spectroscopy: Interpretation based on spectral mixture analysis", in *Remote Geochemical Analysis: Elemental and Mineralogical Composition*, edited by C.M. Pieters and P.A.J. Englert (New York: Cambridge University Press), pp. 145-166.

Blinn, D.W., J.P. Shannon, K.P. Wilson, C.O'Brien, and P.L. Benenati, 1999, "Response of benthos and organic drift to a controlled flood", in *The controlled flood in Grand Canyon* edited by R.H. Webb, J.C. Schmidt, G.R. Marzolf, and R.A. Valdez. American Geophysical Union Geophysical Monograph 110, pp. 259-272.

Boardman, J.W., 1999, "Precision Geocoding of Low-Altitude AVIRIS Data: Lessons Learned in 1998", *Summaries of the Eighth Airborne Earth Science Workshop, AVIRIS Workshop*.

Farrand, W.H., 1992, "A comparison of methods for retrieving apparent surface reflectance from hyperspectral data", *Proc. of the International Symposium on Spectral Sensing Research*, 1154-1164.

Gao, B.C., K.B. Heidebrecht, and A.F.H. Goetz, 1993, "Derivation of scaled surface reflectances from AVIRIS data", *Remote Sens. Environ.*, vol. 44, no. 2/3, pp. 165-178.Howell, E.S., E. Merenyi, and L.A. Lebofsky, 1994, "Classification of asteroid spectra using a neural network", *Journal Geophys. Res*., vol 99, pp 10,847-10865.

Kaplinski, M.K., J.E. Hazel, R. Parnell, and M. Manone, 1999, "Monitoring fine-sediment storage of the Colorado River ecosystem below Glen Canyon Dam, Arizona", *Annual Fact Sheet of the Northern Arizona University Geology Department, Flagstaff, AZ*, 4 p.

Merényi, E., Singer, R.B., and Miller, J.S., 1996, "Mapping of Spectral Variations on the Surface of Mars from High Spectral Resolution Telescopic Images", *Icarus*, vol. 124, pp. 280–295.

Merényi, E., E.S. Howell, A.S. Rivkin, and L.A. Lebofsky, 1997, "Prediction of Water in Asteroids from Spectral Data Shortward of 3 microns", *Icarus*, vol 129, pp 421-439.

Merényi, E., 1998, "Self-Organizing Maps for Planetary Surface Composition Research", Proc. European Symposium on Artificial Neural Networks, Bruges, Belgium, April 22-24, 1998, pp. 197-202. [Downloadable from http://www.lpl.arizona.edu/~erzsebet/emann.html]

Merényi, E., et al, 2000, "Studying the Potential for Monitoring Colorado River Ecosystem Resources Below Glen Canyon Dam Using Low-Altitude AVIRIS Data", *Summaries of the Ninth Airborne Earth Science Workshop, AVIRIS Workshop, February 23-25, 2000, Pasadena, CA, in print*. [Will be downloadable from the AVIRIS web site at http://makalu.jpl.nasa.gov]

NeuralWare, Inc., 1993, "Neural Computing", *NeuralWorks Professional II/Plus, Neural Computing*, NC:293-305.

Rasure , J., and M. Young, 1992, "An Open Environment for Image Processing Software Development, *Proc. Of the SPIE/IS&T Symposium in Electronic Imaging, February 14, 1992*, vol. 1659.

Research Systems Inc., 1997, *ENVI v.3 User's Guide*, RSI, Boulder, 614 pp.

Schmidt, J.C., R.H. Webb, R.A. Valdez, G.R. Marzolf, and L.E. Stevens, 1998, "Science and values in river restoration in the Grand Canyon", *Bioscience* vol 48, pp. 735-747.

Stevens, L.E., 1989, "Mechanisms of riparian plant community organization and succession in the Grand Canyon, Arizona", Northern Arizona University PhD Dissertation, Flagstaff.

Stevens, L.E., J.C. Schmidt, T.J. Ayers, and B.T. Brown, 1995, "Flow regulation, geomorphology, and Colorado River marsh development in the Grand Canyon", *Ecological Applications* vol 5, pp. 1025-1039.

Stevens, L.E. J.P. Shannon and D.W. Blinn, 1997, "Benthic ecology of the Colorado River in Grand Canyon: dam and geomorphic influences", *Regulated Rivers: Research & Management* vol 13, pp. 129-149.

U. S. Department of Interior, Bureau of Reclamation. 1995, "Operation of Glen Canyon Dam, Colorado River Storage Project, Arizona, Final Environmental Impact Statement", U.S. Govt. Printing Office 1995-841:509, Washington, DC.

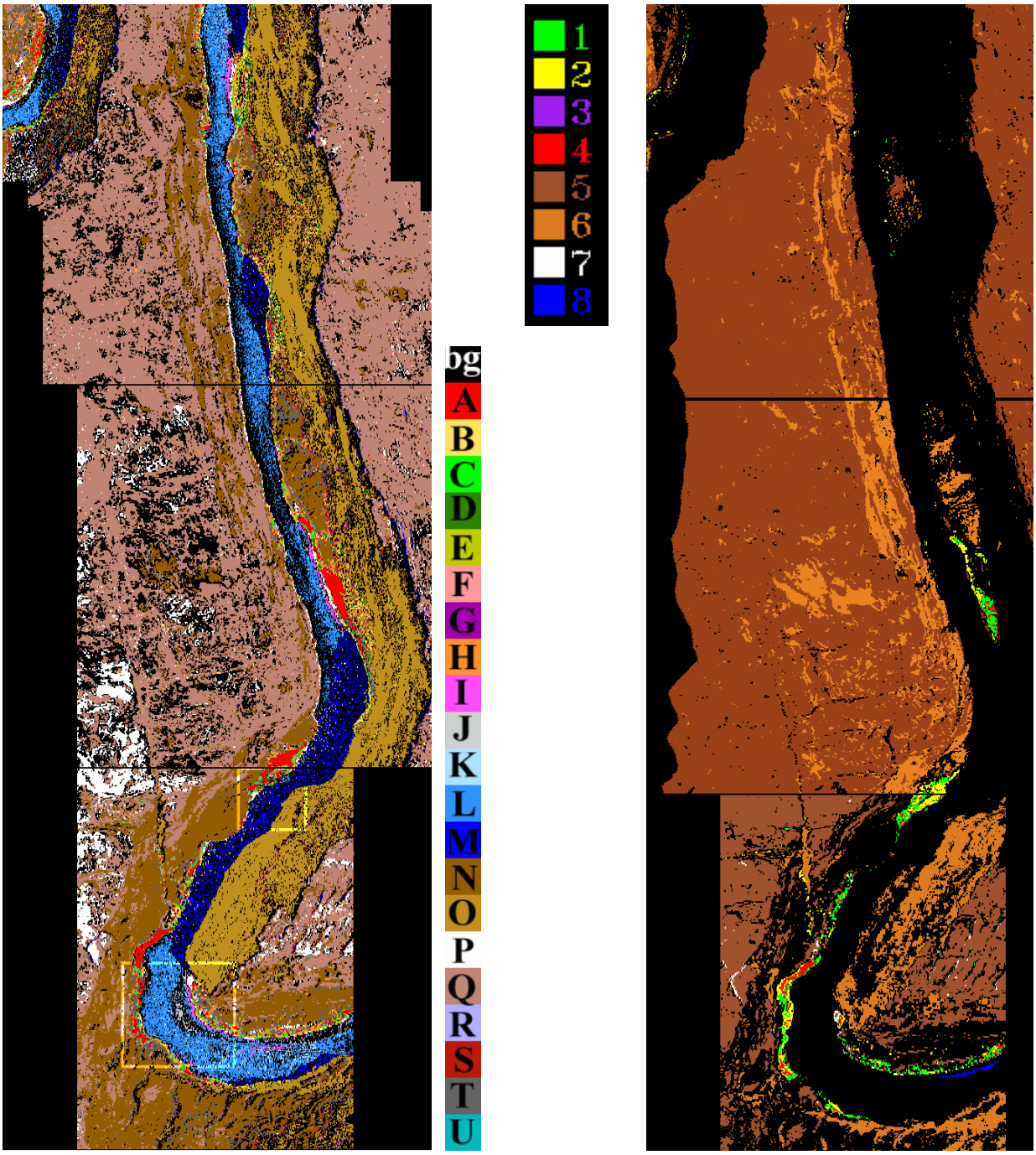

.

Figure 1. Artificial Neural Net and Spectral Angle Mapper classifications. AVIRIS scenes 4, 5 and 6 are shown top to bottom. **1.a (left)** ANN Classification. Bg – Unclassified ; A – Tamarisk; B – Arrowweed, partially decayed; C – Coyote willow; D – Watersedge; E – Mixed grass, green and dry; F – redbud tree; G – Seep willow on sand ridge; H – Grassy talus slope; I – Algae-laden water; J – Submerged sediments 1; K – Submerged sediments 2; L – Submerged sediments 3; M – Deep water and/or very dark shadow, no sediments seen; N – Red sand; O – Red Navaho sandstone; P – White sand; Q – Buff colored Navajo sandstone; R – Unknown; S – upland deciduous mix; T – Sparse vegetation on sand; U – mix of riparian deciduous;
Figure 1.b (right) Spectral Angle Mapper classification of endmembers determined from Spectral Mixture Analysis.
1 – vegetation 1; 2 – vegetation 2; 3 – in-water vegetation; 4 – vegetation 3; 5 – bluff colored Navajo sandstone; 6 – red colored Navajo sandstone; 7 – white sand beach; 8 – submerged sediments.

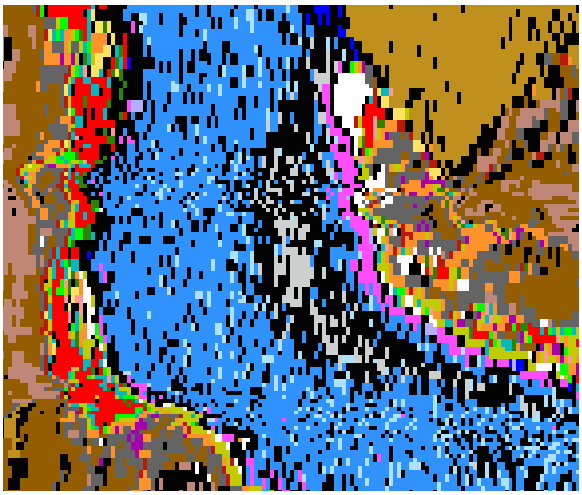

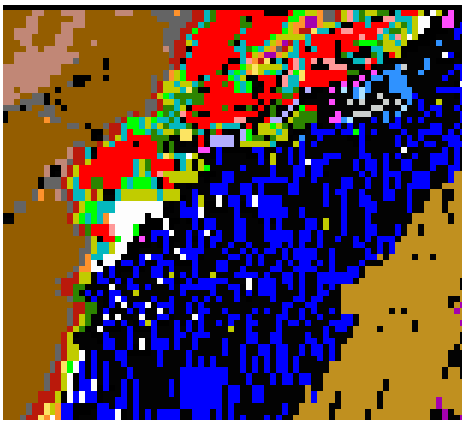

Figure 2.a (left) Enlargement of the lower boxed area in Figure 1.a**. Figure 2.b (Right)** Enlargement of the upper boxed area in Figure 1.a. Both details show systematic zoning of riparian and upland vegetation as well as algae and submerged sediments.

Figure 3. Representative spectra of the species mapped by Artificial Neural Net classification in Figure 1.a. Left: Spectra of vegetation clases. Right: Spectra of "in-water" species and rocks/soils. Spectra have been scaled and offset for optimal viewing.